Research Article

Faten Ermala Che Othman, Norhaniza Yusof, Michael Petrů*, Nik Abdul Hadi Md Nordin, Muhammad Faris Hamid, Ahmad Fauzi Ismail, Ahmad Ilyas Rushdan, and Shukur Abu Hassan

Polyethyleneimine-impregnated activated carbon nanofiber composited graphene-derived rice husk char for efficient post-combustion CO_2 capture

https://doi.org/10.1515/ntrev-2022-0055
received September 26, 2021; accepted January 7, 2022

Abstract: This study presents the fabrication of polyethyleneimine (PEI)–graphene-derived rice husk char (GRHC)/activated carbon nanofiber (ACNF) composites *via* electrospinning and physical activation processes and its adsorption performance toward CO_2. This study was performed by varying several parameters, including the loading of graphene, impregnated and nonimpregnated with amine, and tested on different adsorption pressures and temperatures. The resultant ACNF composite with 1% of GRHC shows smaller average fiber diameter (238 ± 79.97 nm) with specific surface area (S_{BET}) of 597 m^2/g, and V_{micro} of 0.2606 cm^3/g, superior to pristine ACNFs (202 m^2/g and 0.0976 cm^3/g, respectively). ACNF/GRHC0.01 exhibited CO_2 uptakes of 142 cm^3/g at atmospheric pressure and 25°C, significantly higher than that of pristine ACNF's 69 cm^3/g. The GRHC/ACNF0.01 was then impregnated with PEI and further achieved impressive increment in CO_2 uptake to 191 cm^3/g. Notably, the adsorption performance of CO_2 is directly proportional to the pressure increment; however, it is inversely proportional with the increased temperature. Interestingly, both amine-impregnated and nonimpregnated GRHC/ACNFs fitted the pseudo first-order kinetic model (physisorption) at 1 bar; however, best fitted the pseudo second-order kinetic model (chemisorption) at 15 bar. Both GRHC/ACNF and PEI-GRHC/ACNF samples obeyed the Langmuir adsorption isotherm model, which indicates monolayer adsorption. At the end of this study, PEI-GRHC/ACNFs with excellent CO_2 adsorption performance were successfully fabricated.

Keywords: activated carbon nanofibers, carbon dioxide adsorption, graphene-derived rice husk char, nanocomposites, polyethyleneimine

*** Corresponding author: Michael Petrů,** Center for Nanomaterials, Advanced Technologies and Innovations, Faculty of Mechanical Engineering, Technical University of Liberec, Studentská 2, 461 17 Liberec, Czech Republic, e-mail: michal.petru@tul.cz
Faten Ermala Che Othman Advanced Membrane Technology Research Centre (AMTEC), Department of Chemical Engineering, School of Chemical and Energy Engineering (SCEE), Faculty of Engineering, Universiti Teknologi Malaysia, 81310 Johor Bahru, Johor, Malaysia; Centre for Advanced Composite Materials (CACM), Universiti Teknologi Malaysia, UTM Johor Bahru 81310, Johor, Malaysia
Norhaniza Yusof, Muhammad Faris Hamid, Ahmad Fauzi Ismail: Advanced Membrane Technology Research Centre (AMTEC), Department of Chemical Engineering, School of Chemical and Energy Engineering (SCEE), Faculty of Engineering, Universiti Teknologi Malaysia, 81310 Johor Bahru, Johor, Malaysia
Nik Abdul Hadi Md Nordin: Department of Chemical Engineering, Universiti Teknologi Petronas (UTP), 32610 Seri Iskandar, Perak, Malaysia
Ahmad Ilyas Rushdan: Centre for Advanced Composite Materials (CACM), Universiti Teknologi Malaysia, UTM Johor Bahru 81310, Johor, Malaysia; School of Chemical and Energy Engineering, Department of Chemical Engineering, Faculty of Engineering, Universiti Teknologi Malaysia, UTM Johor Bahru 81310, Johor, Malaysia
Shukur Abu Hassan: Centre for Advanced Composite Materials (CACM), Universiti Teknologi Malaysia, UTM Johor Bahru 81310, Johor, Malaysia

1 Introduction

Current dependency on fossil fuel accounts for about 85% of the total global energy production, which contributes to about 40% of the global CO_2 emission. The global monitoring laboratory at Mauna Lao observed an estimated CO_2 weekly average atmospheric concentration of 413.84 ppm during November 2020, 0.78% higher than last year's value and 6.25% higher than the weekly value from 10 years ago [1]. The increased level of atmospheric CO_2 is worrying as it is the major component of the greenhouse gases (GHG) that are a major concern regarding climate change. It is estimated that the global economic damage cause by climate change (including costs associated with climate change-induced market and nonmarket impacts, effects of sea level rise, and consequences associated with large-scale discontinuities) are projected to be $54 and $69 trillion, respectively, relative to 1961–1990 [2].

Therefore, considerable effort has been made by the international community toward reducing the use of these hazardous materials as well as to combat global warming. The most recent realization of the effort was the 21st Conference of Parties (COP21) that was held in Paris, France, in 2015 to limit global temperature rise well below 2°C by the end of this century. In light of the current alarming rate of anthropogenic CO_2 emission, carbon capture and storage (CCS) technologies receive overwhelming attention to combat this issue. These technologies currently serve as reliable mitigation approaches for climate change as well as the key to controlling the global CO_2 emission by controlling the emission of gases from their point source. Through sustainable development along with CCS technology, it is projected that the level of anthropogenic CO_2 emission would be reduced up to 22% of total CO_2 emissions in 2035 [3]. Currently, there are several techniques for CO_2 capture that have been utilized including adsorption, absorption, membrane separation, and cryogenic distillation. Interestingly, adsorption showed great potential due to its economic and easy handling during adsorbent preparation and effective energy consumption for regeneration [4].

A wide variety of adsorbents have been studied over the past decades, such as zeolites [5], silica [6], carbon-based materials [7], and metal organic frameworks (MOFs) [8]. Interestingly, carbon-based adsorbents have aroused intense interest among researchers owing to their tunable pore structure and adjustable surface properties. One example of a newer class of carbon-based sorbents is activated carbon nanofibers (ACNFs), which possess fibrous structure with a large number of active sites and direct accessible micropores for adsorption [9]. Pristine ACNFs have been found to possess moderate specific surface area (S_{BET}) and low carbon yield after the activation process due to high decomposition of polyacrylonitrile (PAN) as the polymer precursor at a high activation temperature. Even though the S_{BET} achieved by ACNFs is moderate, the adsorption capacity of ACNFs is comparable to that of commercial carbon [9]. This is due to the wide range of porosity of the ACNFs with abundant micropores in their structures. The findings from our recent studies [10] have proved that impregnation of nanofillers or additives can improve the physicochemical properties of the adsorbent, especially S_{BET} and porous structure, consequently the adsorption properties.

At present, a number of additive materials are being used, including metal and metal oxides, graphene and graphene oxides (GO), and amine moieties. For instance, ACNFs composited with magnesium oxide (MgO) and showing enhanced porous structure (S_{BET} up to 1,900 m^2/g and 0.7336 cm^3/g) have been successfully synthesized by Othman *et al.* [9]. This approach could be potentially useful in improving their CO_2 adsorption capacity through physisorption. In addition, introducing amine moieties to the adsorbent was also reported to improve CO_2 adsorption capacity *via* chemisorption. Study by Rouzitalab *et al.* [11] demonstrated that N-doped adsorbent enhanced the polarity of the adsorbent surface and significantly improved CO_2 capacity with the adsorption capacity of 7.42 mmol/g at 1 bar. However, regarding the adsorption-based CO_2 separation process, it is well known that, besides the adsorption step, the setup of a reliable and economic sorbent regeneration strategy represents one of the crucial issues to be dealt with. This is because the regeneration mode greatly affects the selection of the most proper reactor configuration, which should be efficient and cost-effective. Currently available regeneration of the sorbent include temperature swing adsorption (TSA), pressure swing adsorption (PSA), vacuum swing adsorption (VSA), and possibly a combination of two modes, for example, hybrid regeneration mode such as VTSA or PTSA [12]. In our previous work, low-cost graphene-derived rice husk char (GRHC) was successfully synthesized and incorporated into the ACNFs [13] and known as GRHC/ACNFs. The GRHC/ACNF composites have shown improvement in S_{BET} and micropore volumes as well as better adsorption capacity. Over these past decades, the carbon-based adsorbents have been further introduced into functional groups that provide basicity to the surface of the GRHC/ACNFs for capturing CO_2. This is because the adsorption performance of CO_2 on the adsorbents is limited due to the low affinity of CO_2 molecules or low moisture toleration as well as limited adsorption at higher temperature (higher than 30°C). To the best of our knowledge, there are no studies available to deliberate on the implementation of polyethyleneimine (PEI) for amine functionalization of the existing GRHC/ACNF adsorbent at the moment. The challenge of amine impregnation is that the amount of amine attached on the surface is limited by the surface area. Therefore, by improving the surface area of the host materials prior to impregnation could potentially elevate their capacity. Thus, this study represents the very first one that extensively discusses the preparation of GRHC/ACNF composites with enhanced properties especially in terms of porosity and impregnation with PEI for excellent postcombustion CO_2 capture.

2 Methods

2.1 Synthesis of graphene-derived rice husk char (GRHC)

GRHC is a graphene-based material that is made from rice husks through a chemical activation method. Rice husks

were procured from a local paddy mill in Kedah, Malaysia. They were chemically treated with potassium hydroxide (KOH; ≥85% pellets) under pure air flow at 200°C to produce rice husk char (RHC). The RHC were ground to form a powder. GRHC were formed by a simple chemical activation method. Details on the synthesis method to convert rice husks into GRHC has been explained in our previous study [14].

2.2 Fabrication of ACNF composites

PAN (M_w 150,000 Da), *N*,*N*-dimethylformamide (DMF), and PEI were purchased from Sigma Aldrich and used as received. PAN and DMF were used to make the polymer dope solution and PEI was used for amine functionalization of the ACNF. Nitrogen gas (99.99%), CO_2 (99.99%), and purified air (99.99%) were acquired from Alpha Gas Solution Sdn Bhd. For the polymer dope preparation, 8 wt% (4 g) of PAN and 92 wt% (46 g) of DMF were used for the total weight of 50 g of solution. Prior to electrospinning, 1 wt% of GRHC relative to PAN was stirred in DMF for a minimum 6 h to form a homogeneous solution and then PAN was added. The dope solution was left stirring for 24 h at room temperature until homogeneity was achieved. The same procedure was repeated with varied GRHC loadings (2.5, 5, 10 g). The composition of all denoted samples are listed in Table 1 with ACNF acting as the control for this study.

The dope solution was then loaded into the electrospinning machine to fabricate the nanofiber. The optimum electrospinning parameters were carried out based on our previous work [15]. The syringe pump was set at 1.0 mL/h, voltage supply at 12 kV, and the needle–collector gap at 15 cm while the environment of the electrospinning chamber was controlled at 30°C temperature and 50% relative humidity. Pyrolysis in a horizontal furnace (model Carbolite 12/65/550) that included three stages, namely stabilization, carbonization, and activation, was carried out next. In the stabilization stage, the NFs were heated up to 275°C under O_2 flow with a heating rate of 2°C/min. Then, carbonization of the stabilized NFs under N_2 atmosphere was carried out with heating up to 600°C (heating rate of 5°C/min) followed by the activation of the carbonized NFs to 800°C (heating rate of 5°C/min), respectively. The gas flow rate and dwelling time used throughout the process were 0.2 L/min and 30 min, respectively.

Table 1: Dope formulation of ACNFs with different graphene loadings of 50 mL solution

Sample name	PAN to graphene ratio	PAN wt (g)	Graphene wt (g)
ACNF	1:0	4	0
GRHC/ACNF0.01	1:0.01	3.96	0.04
GRHC/ACNF0.025	1:0.025	3.90	0.1
GRHC/ACNF0.5	1:0.05	3.80	0.2
GRHC/ACNF0.1	1:0.1	3.60	0.4

2.3 Impregnation of PEI on GRHC/ACNF composites

Amine impregnation was adapted from the study by Khalil and coworkers with some modifications. First, 2 g of ACNFs was mixed with 2 g of PEI and 10 g of DI water. The mixture was magnetically stirred at room temperature for 3 h to make sure the PEI were fully attached on the surface of ACNF samples. Then, the mixture was put into a vacuum oven at 100°C for 5 h for complete drying. A similar procedure was also performed on GRHC/ACNFs. The dried PEI-impregnated samples were further investigated, characterized, and tested for CO_2 adsorption performance.

2.4 Characterization

Before the N_2 adsorption/desorption test, the VacPrep Degasser (VacPrep 061, Micromeritics Instrument Corporation) was used to degas the samples in a processor under vacuum (1×10^{-1} kPa) at 150°C, minimum for 12 h. Then, the textural properties of the porosity of the samples were examined using a porosity analyzer (MicrotracBEL Belsorp-Max) with N_2 (99.9999% purity) at −196°C. The Brunauer–Emmett–Teller (BET) method has been used in determining the specific surface area (S_{BET}), total pore volume (TPV), and mean pore diameter of samples. Meanwhile, the *t*-plot and Barrett–Joyner–Halenda (BJH) methods were used to determine the micropore volume (V_{micro}) of samples. The mesopore volumes (V_{meso}) were evaluated by subtracting the V_{micro} from TPV. In order to study the crystallinity of the materials and their phase structure, X-ray diffractometer (XRD, Rigaku SmartLab) using Cu Kα (λ = 1.54184 Å) at a scanning rate of 1.5°/min was utilized. A Raman spectrophotometer (RMP-510S, Jasco USA) with 514 nm wavelength Ar-ion laser excitation and 20 mW laser power was applied to describe the degree of

graphitization and structural transformation of the samples. The Raman spectrum peaks were recorded within the range of 1,000–3,000 cm^{-1} laser excitation wavelength.

The morphology, structure, and elemental properties and mapping of the samples were conducted with a high-resolution transmission electron microscope (HR-TEM 120 kV; Hitachi HT7700), field-emission scanning electron microscope (FE-SEM), and electron dispersive X-ray (EDX) (Hitachi SU8020; Hitachi Co. Ltd Japan). Prior to characterization, all samples were placed on a copper grid with a carbon film (after ion bombardment) and were left to dry at an ambient atmosphere. Fourier-transform infrared (FTIR, Thermo Scientific/Nicolet iS10) was employed in determining the chemical functionalities in the samples by setting the scanning range of 4,000–1,000 cm^{-1}. For determining the thermal properties of the samples, such as the percentage of carbon yield and weight loss, thermal gravimetric analysis (TGA) (TA Instruments Q600 Simultaneous DSC/TG) was carried out in the range of 25–800°C with a heating rate of 10°C/min under N_2 flow.

2.5 CO_2 adsorption performance

CO_2 sorption was assessed through a volumetric gas adsorption system (Micromeritics TriStar II). Prior to adsorption, all moisture in the samples was firstly removed by degassing the samples for 12 h at 150°C. Each sample with a weight of ±0.1 g was filled into the adsorption column and constant flow of CO_2 (0.015 L/min) was used for the adsorption study. Consequently, samples with the best adsorption performance were subjected to the adsorption test at different temperatures (0, 25, and 50°C) to study their adsorption properties at low to moderate temperatures. As both PEI-impregnated and nonimpregnated GRHC/ACNFs exhibited better adsorption performance over pristine ACNFs, these two samples were used for further assessments including the kinetic and equilibrium characteristics as well as stability studies.

2.6 Kinetics and adsorption equilibrium studies

In order to examine the experimental data of CO_2 adsorption on the ACNF samples at different times, Lagergren's pseudo first-order and pseudo second-order of kinetic models have been employed. According to pseudo first-order characteristics, the adsorption rate is proportional to the number of free adsorption sites on the surface of the adsorbent, and it was calculated based on Equation (1):

$$\ln(q_e - q_t) = \ln q_e - k_1 t \quad (1)$$

where q_e is the weight-specific adsorbed amount of the adsorbate at the end of equilibrium (mmol/g), q_t is the weight-specific adsorbed amount of the adsorbate at time t (s) during the adsorption process (mmol/g), and k_1 is the rate constant of adsorption of the pseudo first-order model.

Thus, it can be assumed that CO_2 adsorption conforms to the pseudo first-order model if the representation of $\ln(q_e - q_t)$ *versus* time can be well fitted to a straight line. Commonly, the pseudo first-order model describes reversible interactions between adsorbates and adsorbent, and therefore indicates physisorption processes [16].

However, according to the pseudo second-order model, the adsorption rate is proportional to the square of vacant adsorption sites as shown by equation (2):

$$\frac{t}{q_t} = \frac{1}{k_2 q_e^2} + \frac{1}{q_e} t \quad (2)$$

where k_2 (mmol/g) is the rate constant of adsorption for the pseudo second-order equation. Consequently, it can be assumed that if the representation of t/q_t *versus* time can be well fitted to a straight line, CO_2 adsorption highly obeys the pseudo second-order model. This model describes relatively strong and chemical interactions between the adsorbents and gas molecules. Thus, the process would be signified by chemical adsorption as the rate-controlling step [17]. Both k_1 and k_2 values were attained from the slopes of the corresponding fitted straight lines.

Similar to kinetic study, only GRHC/ACNFs (PEI-impregnated and nonimpregnated) were used for adsorption equilibrium study. The CO_2 adsorption isotherms show the relationship between the CO_2 adsorbed amount at equilibrium at different pressures (1 and 15 bar). The data obtained were adjusted to the Langmuir and Freundlich models to determine the stages and mechanism of the adsorption of CO_2.

2.7 Regeneration and stability

One of the crucial parameters that need to be considered for the practical application of any adsorbent in the adsorption process is the long-term cycling stability. Therefore, we carried out the desorption of the cyclic CO_2 after each cycle of adsorption to determine the stability of GRHC/ACNFs. In this study, the cycles were repeated five times at the same adsorption conditions in

order to evaluate the regeneration of the GRHC/ACNFs in the early stage. This result will give a better understanding of the adsorbent stability for further use in the following cycles. The cycles were conducted under conditions similar to real-life situations as this temperature is where the CO_2 is stripped out from the flue gas pipe. The regeneration of both exhausted GRHC/ACNFs and PEI-impregnated GRHC/ACNFs was conducted by sweeping the adsorbents with 0.1 L/min upward pure N_2 at 100°C for 5 h. The regenerated adsorbents were reused in an experiment to adsorb CO_2 [18].

3 Results and discussion

3.1 Activated carbon nanofibers composited GRHC (GRHC/ACNF) composites

The N_2 isotherm of all prepared samples are shown in Figure 1, and their microstructure and textural properties are recorded in Table 2. All prepared NF-based materials, including with GRHC shows no microporous structure, (V_{micro} = 0 cm^3/g). After activation, the textural properties of the ACNFs shows the development of meso- and micropores and increment in the surface area. Type I(b) isotherms derived from the N_2 adsorption/desorption in Figure 1 explains the microporous attributes in all ACNF samples. [19,20]. Typical adsorption response of microporous materials can be seen from the stagnant plateau isotherm of all the ACNFs at p/p_0 = 0.05–0.95; however, above 0.95 the adsorption curve continually increases. Additionally, as Qi *et al.* [19] suggested, H3-type of hysteresis loop was observed from the N_2 adsorption/desorption isotherms (p/p_0 = 0.4–1.0), which was due to the capillary condensation in the mesoporous pores [21,22]. It is confirmed that all the activated samples were mainly microporous with a high proportion of V_{micro} in relation to the TPV as shown in Table 2. Along with it, the values of V_{meso} indicating the proportion of mesoporous structure are also tabulated.

At an activation temperature of 800°C, it can be significantly observed that S_{BET} increases in all ACNF samples as shown in Table 2, which represents the formation of mesoporous/microporous structures. This could possibly be due to the catalytic effects of GRHC that takes place at higher temperatures [23]. For example, the S_{BET} of ACNF drastically improved from 17 m^2/g to 139 m^2/g after the activation. Prior to activation, it can be seen that the S_{BET} is very low in all samples, and it is considered that there is no significant catalytic ability at low temperatures. The S_{BET} considerably increases after activation indicating that GRHC has good catalytic ability for creating porosity at higher temperature. Interestingly, the highest S_{BET} of 597 m^2/g was measured for GRHC/ACNF0.1 while further increasing GRHC loading diminished its textural properties. As shown in Table 2, ACNFs with the highest loading of GRHC show the lowest S_{BET} and V_{micro}. Importantly, the adsorbents with high S_{BET} and V_{micro} are preferable as these are important factors for the adsorption of gas

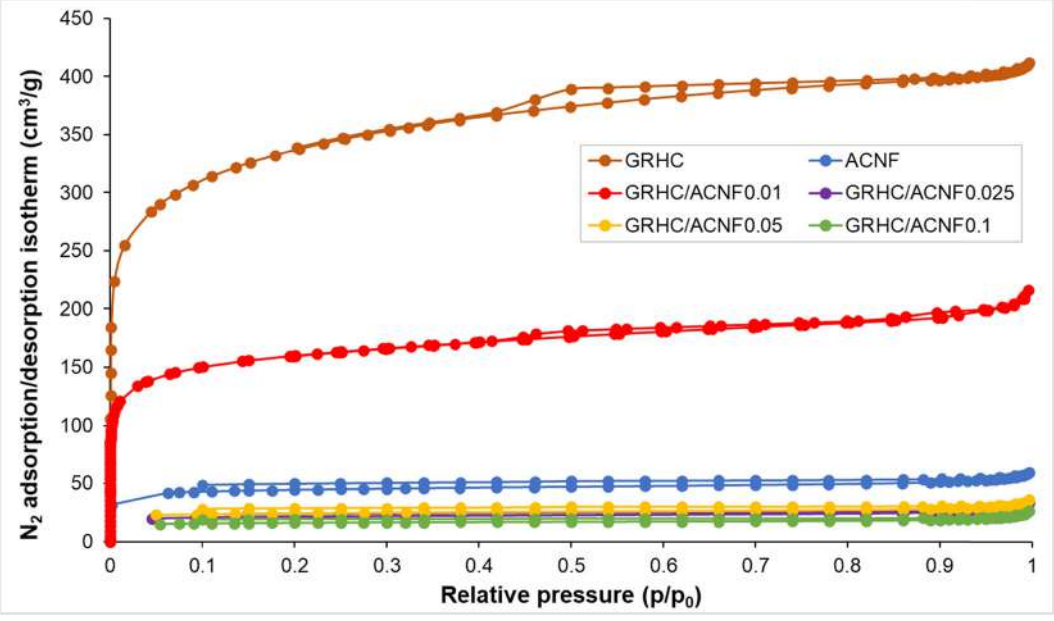

Figure 1: N_2 adsorption/desorption isotherms of ACNFs synthesized at different loadings of GRHC after activation.

Table 2: Porous structure characteristics of pristine and composite ACNFs prior and after activation

	Samples	S_{BET} (m^2/g)	TPV (cm^3/g)	V_{micro} (cm^3/g)	V_{meso} (cm^3/g)	DP_{Ave} (nm)
Prior activation	NF	17.17	0.1364	0	0	31.7692
	GRHC/NF0.01	17.80	0.1423	0	0	31.9677
	GRHC/NF0.025	18.24	0.0053	0	0	21.0940
	GRHC/NF0.05	57.71	0.4284	0	0	29.6902
	GRHC/NF0.1	15.80	0.0796	0	0	20.1624
After activation	ACNF	138.67	0.0930	0.0548	0.0382	2.8424
	GRHC/ACNF0.01	597.27	0.3218	0.2606	0.0612	2.174
	GRHC/ACNF0.025	66.41	0.0523	0.0267	0.0256	3.3385
	GRHC/ACNF0.05	78.26	0.0562	0.0309	0.0253	2.8728
	GRHC/ACNF0.1	51.65	0.0412	0.0205	0.0207	3.1897

S_{BET} = specific surface area; TPV = total pore volume; V_{micro} = micropore volume; V_{meso} = mesopores volume; DP_{Ave} = Average pore diameter.

molecules [24]. The V_{meso} increases and V_{micro} decreases with the increasing loading of GRHC. This increment of GRHC loading leading to poor textural properties of the ACNF composite could possibly be due to the effects of high conductivity of GRHC that could interfere with the jet ejection during electrospinning for producing nanofibers with larger diameter and formation of beads that results in pore blockage (see Supplementary Materials, Figure S1).

The XRD spectra of all samples in this study are shown in Figure 2. For GRHC, a sharp peak at 28.6° representing the (002) lattice plane and a broad peak at range 17°–31° representing hexagonal graphite were observed. All ACNFs shows two diffraction peaks ranging between 17°–31° and 41°–43°, representing hexagonal graphite and rhombohedral graphite, respectively [25], with variation only in their intensities. Peaks appear around 17°–31° corresponding to the (002) plane of the carbon skeleton [25]. This represents the formation of ladder structures within the ACNF and the composites after the cyclization of PAN activation. Moreover, XRD analysis reveals their crystallographic (100) and amorphous (110) planes [26]. Apparently, the presence of the low and broad peaks in the range of 41°–43° indicates that samples have amorphous structure and possess very low graphitization degree. This finding corresponds well to the one obtained by Raman spectroscopy. All amorphous ACNFs obtained in this study could possibly be due to the destruction of the in-plane aromatic lattices [27], leaving a large number of defect structures in the ACNFs [28,29]. Remarkably, there is no appearance of the GRHC peak in all ACNF composites and this is believed to be due to the very small amount of GRHC used in all composite samples, which is below 10% (relative to PAN wt) that contributed to very weak peak or insignificant peak in the amorphous structure of the carbon materials. In 2012, Guo *et al.* [30] found that the carbon materials with amorphous and defective structures were considered to have greater ability in modifying the textural characteristics of the ACNFs, which was also observed in this study (Figure 1 and Table 2).

Raman spectroscopy was used in this study to identify the structural features and degree of graphitization of the GRHC and pristine ACNFs, as well as their composites, as shown in Figure 3. All activated samples exhibited two distinguishing peaks, which are at 1,368 cm^{-1} and 1,612 cm^{-1} but with different intensities. These two peaks indicated the appearance of the D-band and G-band of graphitic materials in the samples, respectively. In conjunction, the D-band spectra of all samples stipulated the existence of defective and amorphous carbon structure whereas the presence of the G-band signified the orderly structure of the graphene with sp^2 hybridization of the carbon atom. The intensity is relatively high at a low loading of GRHC (1 wt%), and further increasing the loading diminishes their intensity.

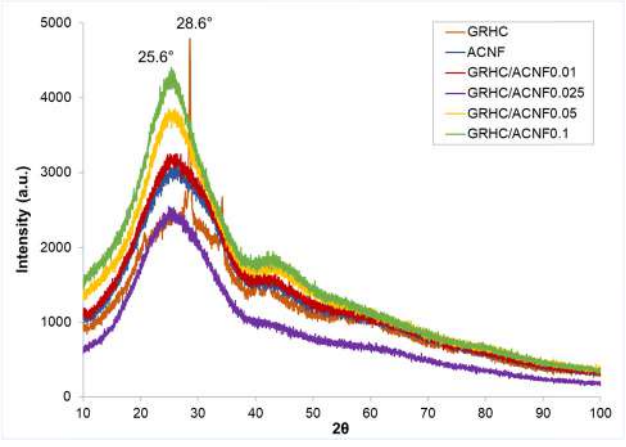

Figure 2: XRD spectra of GRHC, pristine, and composite ACNFs with different loadings of GRHC.

As mentioned in previous literature, the formation of the graphene material can be confirmed from the appearance of the 2D-band spectrum around 2,700 cm^{-1} of the Raman shift [31]. Broad and weak 2D-bands around 2,700–2,800 cm^{-1} can be observed in all ACNF samples in Figure 3. The very low intensity of the 2D-band in ACNF composites is believed to be due to too small amount of GRHC composited into the structures. It is worth noting that all ACNF-based samples exhibited defect structures and highly amorphous nature as indicated by the intensity of the D-band being higher than the G-band, concurring with the XRD result analysis. In contrast, the G-band is higher than the D-band in the GRHC sample proving its higher crystallinity as a graphene-based material.

Pristine GRHC exhibits the smallest intensity ratio $R(I_D/I_G)$ of 0.96 for D-band to G-band among all materials under investigation due to the ordered carbon structures as well as the high degree of graphitization [32,33] whereas ACNF exhibits $R(I_D/I_G)$ of 1.35 indicating a highly disordered structure. Incorporating GRHC into the ACNF shows the composite structure becoming more ordered as implied by the decrease in $R(I_D/I_G)$ with increasing GRHC, with exception of GRHC/ACNF0.01. It shows that $R(I_D/I_G)$ of GRHC/ACNF0.01 is higher than that of pristine ACNF and this is corresponding well with the BET and XRD results discussed earlier, indicating this sample possesses the most disordered structures. As more GRHC was incorporated into ACNFs, the composites became more ordered and this could be explained by the addition of the highly ordered structure of pristine GRHC that could affect the structure of the composites.

The graphitic structure of the GRHC/ACNF composites is expected to diminish with the increment of GRHC loading. Regardless of its lowest $R(I_D/I_G)$ in comparison with other ACNF composites, the carbon material with this value is believed to possess disordered and defective structures. This is validated by Gayathri *et al.* [31], who found that the graphene synthesized in their research still possessed defect structure even at a significantly low value of $R(I_D/I_G)$ of ~0.2–0.4. Remarkably, in this study, their defective structures are more preferable for better gas adsorption due to porosity enhancement caused by the defects. This means the sample with higher $R(I_D/I_G)$, such as GRHC/ACNF0.01, will show better performance toward CO_2 adsorption.

Figure 4 shows the morphological structure of the ACNF at different magnifications and loadings and summarized in Table 3. The development of the porous structure after the activation of the NFs was proved with the appearance of pores on the ACNF structure as shown in Figure 4(e). Among all samples, GRHC/ACNF composited with 1% of GRHC exhibited the smallest fiber diameter of 238 ± 79.97 nm as shown in Table 3. Bead formation was observed in ACNF composites likely due to conductive properties provided by the GRHC and the viscosity of the solution [34]. This would affect the final diameters of the fibers due to the electrostatic repulsion within the jet spray from the tip of the needle to the collector surface throughout the electrospinning process. Huang *et al.* [35] reported that high conductivity led to the production of electrospun fibers with smaller diameter due to the increment of the surface tension of the solution, which affects the jet ejection during electrospinning. Thus, it can be hypothesized that increasing GHRC loading would result in a smaller diameter. However, interestingly in this study, only GRHC/ACNF0.01 resulted in the smallest diameter whereas

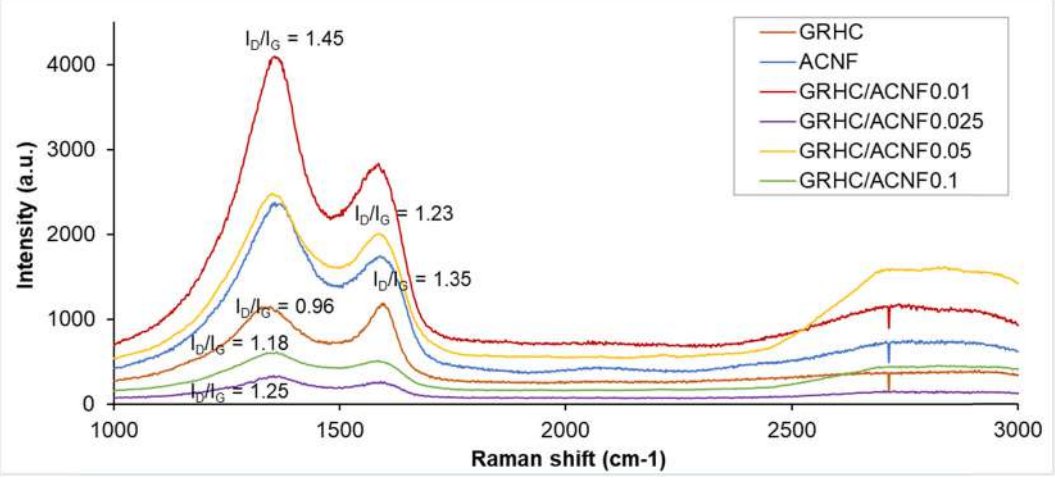

Figure 3: Raman spectra of GRHC, pristine, and composite ACNFs with different loadings of GRHC.

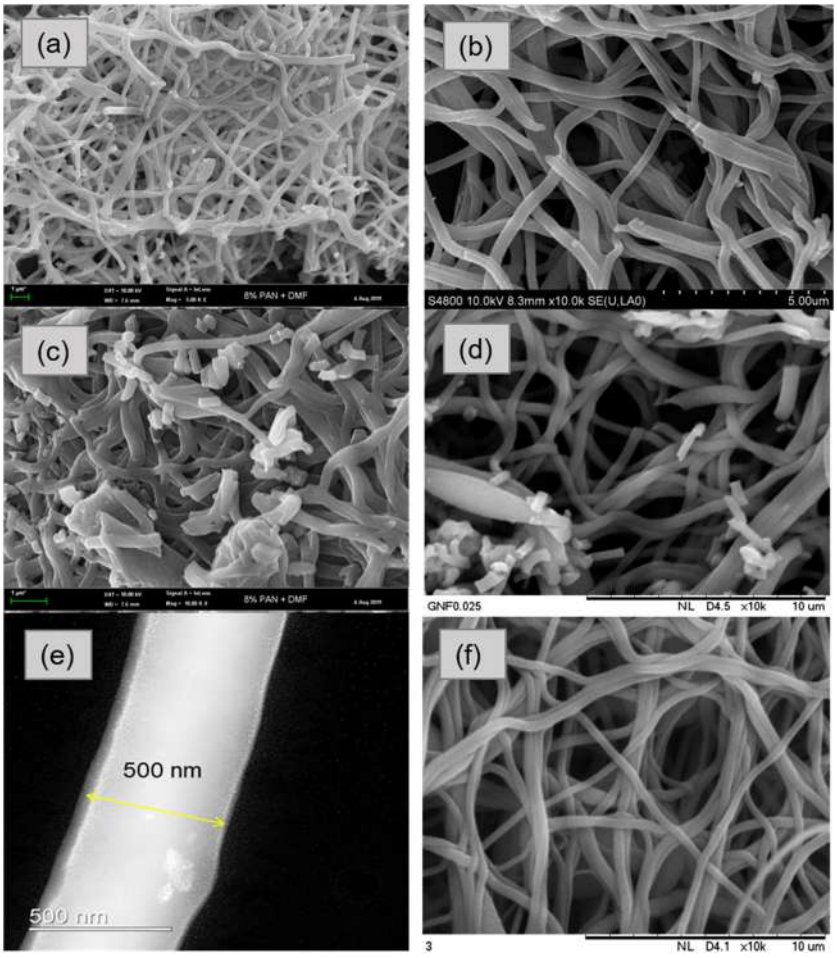

Figure 4: FE-SEM images of pristine ACNFs at different magnifications: (a) 5,000×; (c) 10,000×; (e) 100,000×; and with different loadings of GRHC at 10,000× (b) GRHC/ACNF0.01; (d) GRHC/ACNF0.05; (f) GRHC/ACNF0.1.

increasing GHRC loading further increases the fiber diameter (albeit smaller than ACNF). The results show correlation with the S_{BET} obtained (Table 2) where smaller diameter provides higher S_{BET} and vice versa. From the results obtained, only GRHC/ACNF0.01 has been used for further impregnation study and pristine ACNF has been used for comparison.

Moreover, another major point to be addressed in this study is the particle size of the GRHC/ACNF0.01 in powdered form. From the results of this current study (see Supplementary Materials, Figure S2), the average particle size of GRHC/ACNF obtained ranged from 22.2 to 35.4 μm. Compared with other sorbents, this range of particle size is a good indicator of the suitability of these samples as good sorbents. It is believed that the size of the particles can greatly affect the adsorption properties of the sorbents. This was supported by a study conducted by Li *et al.* [36] as they found that particle size of 52.5 μm or smaller resulted in higher absorption of CO_2 as compared with a particle size of 77.5 and 100.0 μm. Even though this sorbent has been ground into powdered form, however, under high magnification image, the thread-like structure of the nanofibers remains as shown in Figure 4.

In terms of mechanical strength, this proposed GRHC/ACNF is believed to possess good mechanical strength, including high tensile strength, which could be due to

Table 3: Diameter of the pristine and composite ACNFs at different loadings of GRHC

Sample	Average diameter (nm)	Standard deviation (nm)
ACNF	460	±57.05
GRHC/ACNF0.01	238	±79.97
GRHC/ACNF0.025	296	±40.58
GRHC/ACNF0.05	340	±57.05
GRHC/ACNF0.1	384	±52.87

the highly oriented fibers during the electrospinning process that affect the mechanical strength of the nanofibers. Due to limitations of time limitation and availability of instruments, the mechanical test on the GRHC/ACNF could not be conducted. However, superiority of the mechanical properties possessed by GRHC/ACNF can be seen from similar materials such carbon nanofibers studied in several previous work reviewed by Yadav *et al.* [37]. For example, Pu *et al.* [38] have successfully fabricated electrospun carbon nanofibers with excellent mechanical properties, such as high tensile strength up to 20.7 MPa. According to their studies, the stretching effect of the jet during electrospinning is advantageous to the arrangement of carbon nanofibers along the fiber axis, which significantly enhances the tensile strength and modulus of the fibers [38].

3.2 PEI-impregnated ACNFs and GRHC/ACNFs

Figure 5 shows the N_2 adsorption/desorption isotherms of PEI-impregnated ACNFs and GRHC/ACNF0.01. Both impregnated samples exhibit similar type of isotherm, which is type II indicative of nonporous or macroporous structures [39]. The isotherm type changes from type I(b) prior to activation into type II after activation. This type of isotherm explained the formation of a monolayer at relatively low pressure, and then multilayer formation at higher relative pressure [40]. In contrast with the type I isotherm, the long plateau is absent in type II isotherm as the adsorption uptake continuously increases with the relative pressure without significant halt and it even almost reaches unity, indicating the multilayer adsorption.

Table 4 summarizes the corresponding textural properties of both impregnated samples. As compared with nonimpregnated samples, both PEI-impregnated samples have shown significant reduction in S_{BET} and TPV, with the disappearance of V_{micro} in the structure. This reduction of S_{BET} confirms that PEI was successfully impregnated onto the porous structures of the ACNF samples, and all of its porosity structure was filled with PEI. Rouzitalab and coworkers have reported that adsorbent materials that are high in TPV were easily accessible by the N-functional groups, which results in blocking the pores of the ACNFs, and were reflected by the decrement of the S_{BET}. In this case, the physisorption that mainly depends on S_{BET}, which predominantly lay in its pores, would be mostly excluded and chemisorption takes place.

The thermal stability of the impregnated ACNFs was evaluated using TGA analysis in the temperature range of 25–700°C (Figure 6). All impregnated ACNFs exhibit thermal decomposition at a higher onset temperature of ~400°C. This result suggests PEI-impregnated ACNFs have better thermal stability as compared with nonimpregnated samples. From the thermogram, the weight

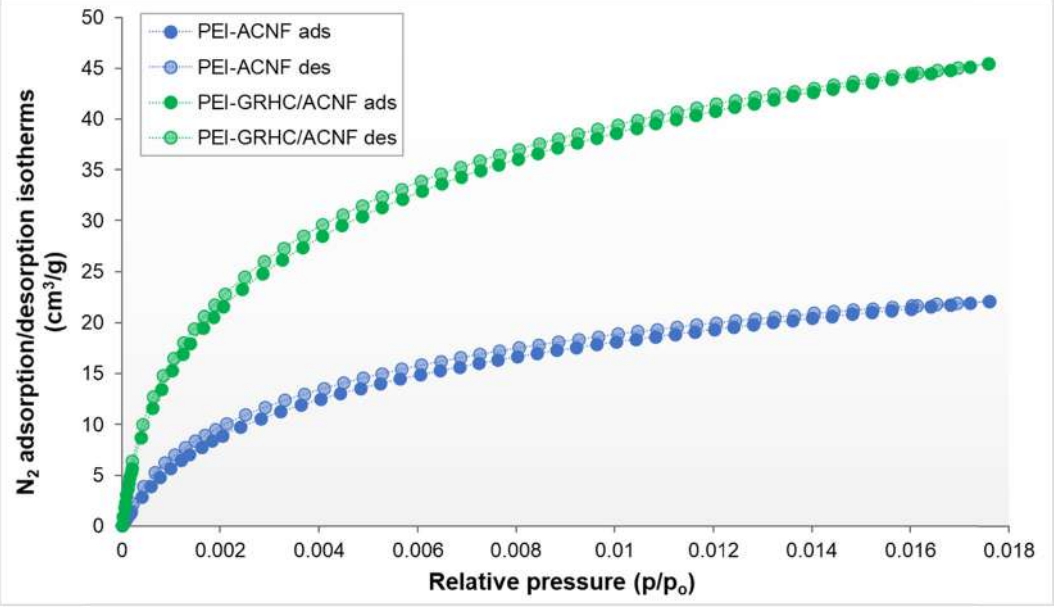

Figure 5: N_2 adsorption/desorption isotherms of PEI-impregnated ACNFs and PEI-impregnated GRHC/ACNFs.

Table 4: Textural characteristics of PEI-impregnated ACNFs and GRHC/ACNFs

Samples	S_{BET} (m^2/g)	TPV (cm^3/g)	V_{micro} (cm^3/g)	DP_{ave} (nm)
PEI-ACNF	2.5162	0.0052	0	8.3243
PEI-GRHC/ACNF	1.9032	0.0043	0	9.1175

percentage of the ACNFs improved from 24.2% to 36.2% as compared to PEI-ACNF. Meanwhile for PEI-impregnated GRHC/ACNFs, the final weight obtained is much higher than the nonimpregnated one, which is up to 68.2%. This is could possibly be due to the low volatility and good stability properties of PEI [41]. This result is expected to contribute to GRHC/ACNF stability and cyclability during the real-life flue gas separation in postcombustion CO_2 capture.

Figure 7 exhibits the FTIR spectra of the nonimpregnated and PEI-impregnated ACNFs and GRHC/ACNFs, respectively. Compared with nonimpregnated ACNFs. A broad band at 2,980 cm^{-1} was observed, which indicates the existence of $-CH_2$ symmetric stretching modes of the PEI chain in the PEI-impregnated samples. The band at 1,557 cm^{-1} also can be observed in all impregnated samples associated with the asymmetric bending of the primary amines ($-NH_2$). The appearance of this peak further supports successful impregnation of PEI [42,43].

The SEM, TEM images, and EDX mapping of PEI-impregnated GRHC/ACNFs is presented in Figure 8(a)–(d). As shown in Figure 8(a), it can be seen that the morphology of PEI-GRHC/ACNF was agglomerated with appearance of large beads, which is believed happened during the impregnation process. The presence of black spots within the fibers in Figure 8(b) indicates the GRHC presence onto the structures. Furthermore, the presence of a small amount of silica (0.02 ± 0.02 wt%) in the nanowires was also observed [44] in Figure 8(c). This also can be seen with the appearance of silica in the resultant GRHC/ACNFs through EDX mapping (Supplementary Materials, Figure S3), which indicating the high content of silica in untreated (raw) rice husks (prior conversion into GRHC). Through EDX analysis, Table 5 confirms the existence of a high concentration of N atoms on the impregnated samples (35.21 ± 6.81 wt%). The other major elemental properties such as carbon (C) and oxygen (O)

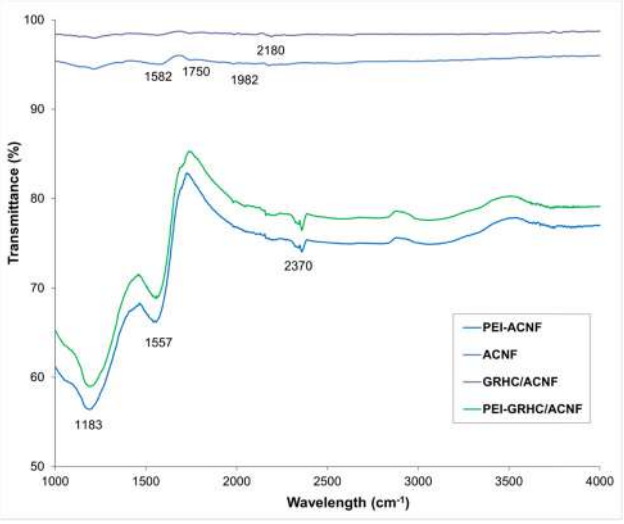

Figure 7: FTIR spectrum of PEI-impregnated and nonimpregnated ACNFs and GRHC/ACNFs.

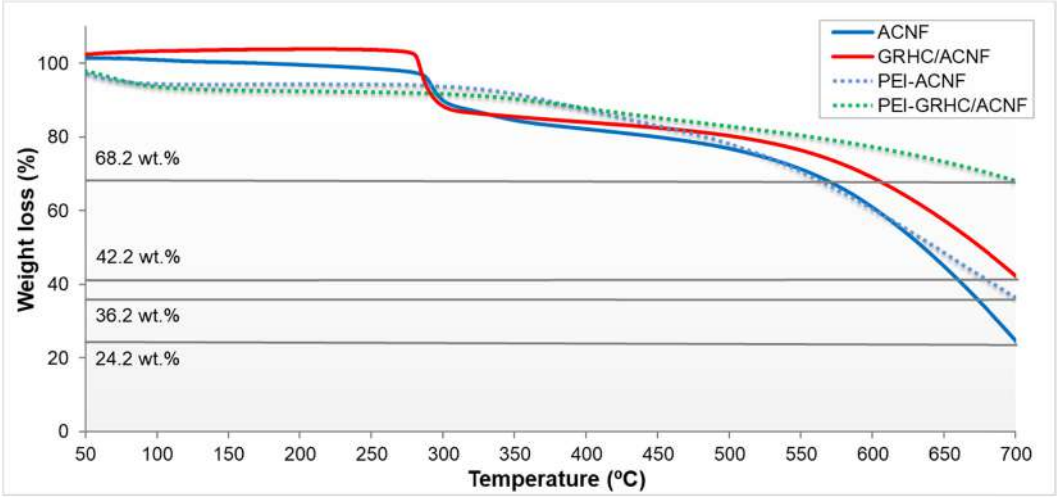

Figure 6: TGA thermogram of PEI-impregnated and nonimpregnated ACNFs and GRHC/ACNFs.

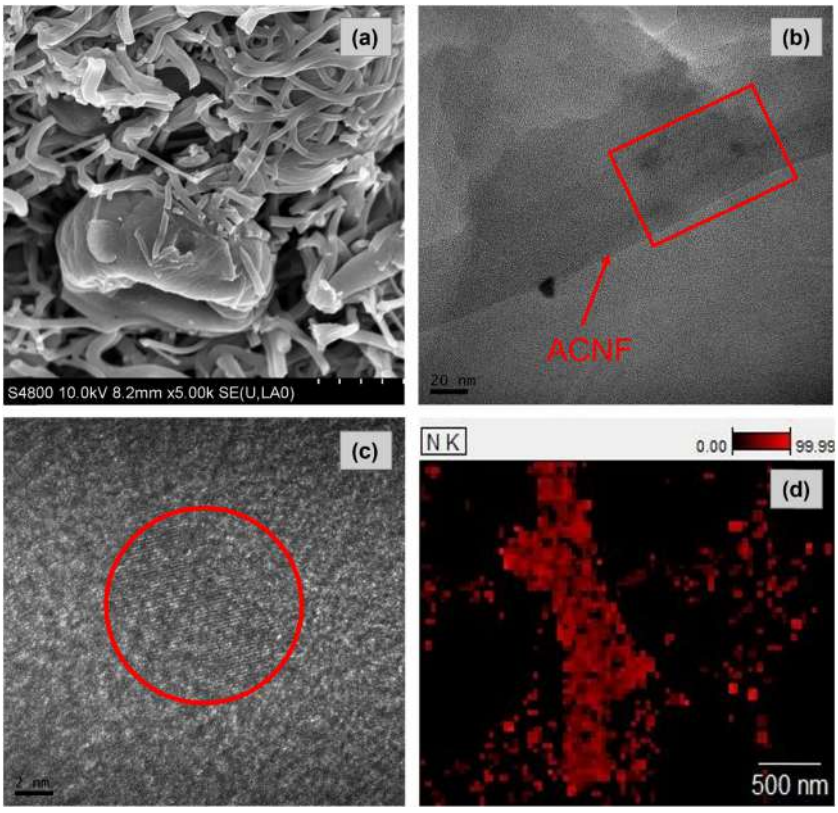

Figure 8: (a) SEM image at magnification of 5,000×; (b and c) TEM images at different magnifications; and (d) EDX mapping of PEI-impregnated GRHC/ACNFs.

were also detected at 51.45 ± 0.74 wt% and 13.32 ± 1.71 wt%, respectively. As expected, C covers the highest percentage among other elements as ACNFs are carbon-based materials.

3.3 Adsorption performance and characteristics toward CO_2

GRHC/ACNFs showing better CO_2 adsorption than the pristine ACNFs (Figure 9) at pressure 1–15 bar indicate that the presence of graphene improves its affinity toward CO_2 as it contributes to the enhancement of the textural properties of the adsorbents [45]. These results are in agreement with the BET results where higher S_{BET} and V_{micro} [46] provide more surface for gas to be adsorbed. Compared with other previous works, both ACNFs possess higher CO_2 adsorption compared with other carbon-based materials as summarized in Table 6, even though with lower S_{BET} values. It is believed that the high adsorption value is not totally S_{BET} dependent, yet it also could be contributed by the available open micropores on the adsorbents. For example, most of the CNF-based adsorbents in Table 6 showed higher S_{BET} as compared with the samples in this study, however, with lower V_{micro} values and limited CO_2 adsorption capacities. This means V_{micro} is a very important characteristic for adsorbents to adsorb higher gas. From this, it can be seen that the resultant ACNFs can be good candidates for gas adsorbents, especially in flue gases, in order to reduce the CO_2 emission into the atmosphere, consequently combating the global warming problem.

Various sorbent materials have been widely used in current adsorption technology and further assessment on their performance needs to be clarified. Table 7 shows the comparison of the sorbents' properties and their adsorption capacities to further assess the potential of currently synthesized GRHC/ACNFs compared with other available sorbent types, such as conventional activated carbon,

Table 5: Elemental properties of PEI-impregnated GRHC/ACNFs

Element	Weight (%)	Wt% error	Atom%	Atom% error
C	51.45	±0.74	56.13	±0.80
N	35.21	±6.81	32.95	±6.39
O	13.32	±1.71	10.91	±1.42
Si	0.02	±0.02	0.01	±0.01
Total	100.00		100.00	

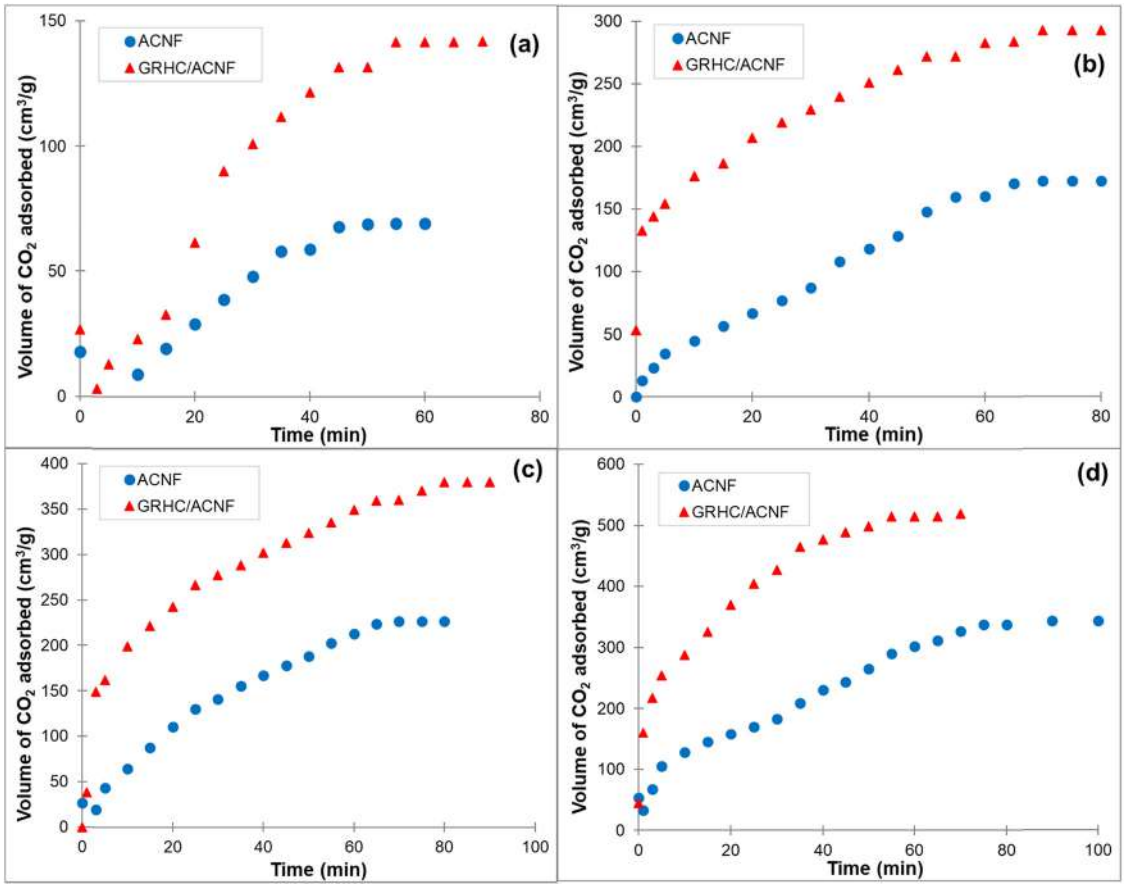

Figure 9: CO_2 adsorption of ACNFs and GRHC/ACNFs at different adsorption pressures: (a) 1 bar; (b) 5 bar; (c) 10 bar; (d) 15 bar at 25°C.

zeolites, carbon nanotubes (CNTs), MOFs, graphene, and so on. Among the available adsorbents, carbon-based adsorbents have shown promising adsorption performance as excellent gas adsorbents due to their large surface area and availability (can be produced from wide range of raw materials). In the past few decades, activated carbon is the commonly used adsorbent in various applications. The wide utilization of activated carbon in adsorption industries is advantageous due to their wide distribution of pore structures and surface chemistry for gas adsorption. Most importantly, activated carbon is relatively low in cost, has high S_{BET}, widely available, has an easily modifiable pore structure, , susceptible to surface functionalization, and can be regenerated [53,54].

Recently, activated carbon has been obtained in different structures and forms, including powder, granular, tubular, and fibers. It was found that activated carbon in fiber form has shown significant structure improvement,

Table 6: Comparison of CO_2 adsorption capacity on various types of carbon fibers and their composite-based adsorbents

Adsorbent	S_{BET} (m^2/g)	V_{micro} (cm^3/g)	Vol. of CO_2 adsorbed (cm^3/g)	Temp; pressure	Ref.
ACNF	139	0.06	69	25°C; 1 bar	This work
GRHC/ACNF	597	0.32	142	25°C; 1 bar	This work
CNF-SnO_2	434	0.20	58	25°C; 1 atm	[34]
CNF-MIL-53	140	—	30	25°C; 1 bar	[47]
PAN-CMFs	966	—	64	25°C; 1 bar	[48]
Graphite NFs	567	0.27	59	25°C; 1 atm	[49]
Graphite NFs	966	0.25	71	25°C; 1 atm	[50]
$NiCo_2O_4$/CNTs CNFs	40	—	34	25°C; 1 bar	[51]
Phenolic resin-based carbon ultrafine fibers	650	—	65	25°C; 1 bar	[52]

Table 7: Comparison of various types of available sorbent materials

Adsorbent	S_{BET} (m^2/g)	Pore volume (cm^3/g)	Temperature; pressure (°C; bar)	Volume adsorbed (cm^3/g)	Ref.
GRHC/ACNF	597	0.32	25°C; 1 bar	142.0	This work
MCM-41	1211	1.3	—; 1	99.9	[56,57]
Mesoporous alumina	812	0.83	—; 1	115.4	[58]
Activated carbon	2187	0.82	25; 8	24.4	[59]
13X-zeolites	710	—	120; 20	15.5	[60]
Microporous polymers	1237	—	25; 1	48.8	[61]
Porous clay heterostructures	640	0.828	25; 1	14.2	[62]
Graphene	443	—	25; 11	47.9	[29]
Carbon nanotubes	60	0.4	25; 1.1	155.3	[63]
Coconut shell-based AC	378	—	35; 1	13.8	[64]
Pitch-based AC	1053	—	28; 20%	42.6	[65]
Activated carbon fibers (ACF)	1256	0.636	30; 0.05%	0.08	[66]
Carbon molecular sieve	857	0.501	30; 0.05%	0.36	[66]
ACFs (physical activation)	1,240	0.61	30; 1.1	146.1	[67]
ACFs (chemical activation)	2,180	1.003	30; 1	126.1	[68]
Graphene sheets	484	0.682	0; 1	64.2	[69]
Rice-husk char	1,041	0.53	0; 1	125.0	[70]
Graphite nanofibers	567	0.708	25; 1.01	30.0	[49]

especially in terms of surface area, micropores, active site availability, and gas adsorption capacity as compared with the traditional granular form [55]. The presence of fibril structure in ACNFs has ensured much higher adsorption capacity, which is due to the direct diffusion of gas adsorbates into the available micropores inside and on the surface of the adsorbents. This means there is no resistance for adsorbates to reach the adsorption sites as there are no macropore or mesopore network. Moreover, this fiber form can be prepared from a wide range of precursors such as coal, polymers, petroleum pitch, rayon, and viscose.

As listed in Table 7, the adsorbed volume of CO_2 by the ACF and GRHC/ACNF are the highest, which are 6.4 and 6.58 mmol/g, respectively compared with other adsorbents. Even though, the CO_2 adsorbed volume is comparable for both samples, the S_{BET} value is significantly different, which is 1240 m^2/g for ACF and 597 m^2/g for GRHC/ACNF. From this finding, it can be concluded that even at low S_{BET} value, the adsorption performance of the as-proposed adsorbent, GRHC/ACNF, is better than that of the other mentioned adsorbents. It is believed that tuning into higher S_{BET} value can potentially turn this GRHC/ACNF into an excellent CO_2 adsorbent. Besides S_{BET} value, another important factor that affects the adsorption performance is the compatibility of the adsorbents for real-life CO_2 capture applications. As mentioned in the TGA results above, GRHC/ACNF with good thermal stability (up to 700°C) can withstand the temperature during postcombustion CO_2 capture ranging from 40°C to 80°C, which makes this proposed GRHC/ACNF as one of the excellent CO_2 adsorbents.

The CO_2 adsorption performance of PEI-impregnated GRHC/ACNFs is presented in Table 8. The CO_2 adsorption capacity was higher at 107 cm^3/g for PEI-ACNFs (55% enhancement) and 191 cm^3/g for PEI-GRHC/ACNFs (34% enhancement) as compared with their nonimpregnated samples, which were 69 cm^3/g and 142 cm^3/g for ACNFs and GRHC/ACNFs, respectively. This has proved the involvement of chemical interaction between the basic N-functionalities in PEI and acidic CO_2 molecules. From this finding, it is believed that the high adsorption capacity in PEI-impregnated samples could be contributed by the involvement of both physical and chemical interactions between the adsorbent and adsorbates.

In terms of adsorption in more practical dynamic conditions in multicomponent mixtures such as flue gases, this newly produced both impregnated and nonimpregnated GRHC/ACNFs are believed to have good gas separation

Table 8: CO_2 uptakes at different pressures at ambient temperatures

Sample	CO_2 uptakes (cm^3/g)				
	PEI-1 bar	1 bar	5 bar	10 bar	15 bar
ACNF	107	69	173	242	293
GRHC/ACNF	191	142	342	413	522

properties. This statement was made by considering and comparing the N_2 adsorption obtained from BET results and the CO_2 adsorption capacity. From BET results, the PEI-impregnated sample shows very low N_2 adsorption capacity of 2.67 cm^3/g whereas the nonimpregnated sample possesses higher adsorption capacity of 33.7 cm^3/g. The low N_2 adsorption on PEI-GRHC/ACNFs indicates the blockage of the available porous structure (very low S_{BET} as previously discussed) by PEI for N_2 molecules to be adsorbed onto the structure. As N_2 is an inert gas, it does not interact with N-functionalities on the surface of PEI-GRHC/ACNFs. In contrast, the nonimpregnated sample exhibits higher N_2 adsorption due to the numerous available porous structures, which contributes to physisorption. According to both N_2 and CO_2 adsorption capacity, it is believed that the resultant GRHC/ACNFs more selective toward CO_2. From this finding, GRHC/ACNFs can potentially act as a good adsorbent for flue gas separation in postcombustion CO_2 capture.

As previously discussed, the GRHC/ACNFs possessed the highest S_{BET} and TPV prior to PEI impregnation but the lowest after impregnation. It can be attributed to the presence of amine in the GRHC/ACNFs. This phenomenon explains the high CO_2 adsorption capacity in PEI-GRHC/ACNFs even though they possessed smallest values of S_{BET} and TPV as compared with GRHC/ACNFs, which is highly believed to be influential in both physisorption and chemisorption. In conclusion, it can be said that high CO_2 adsorption capacity in PEI-GRHC/ACNFs is attributed to a synergic effect of amino groups, thus multiplying the

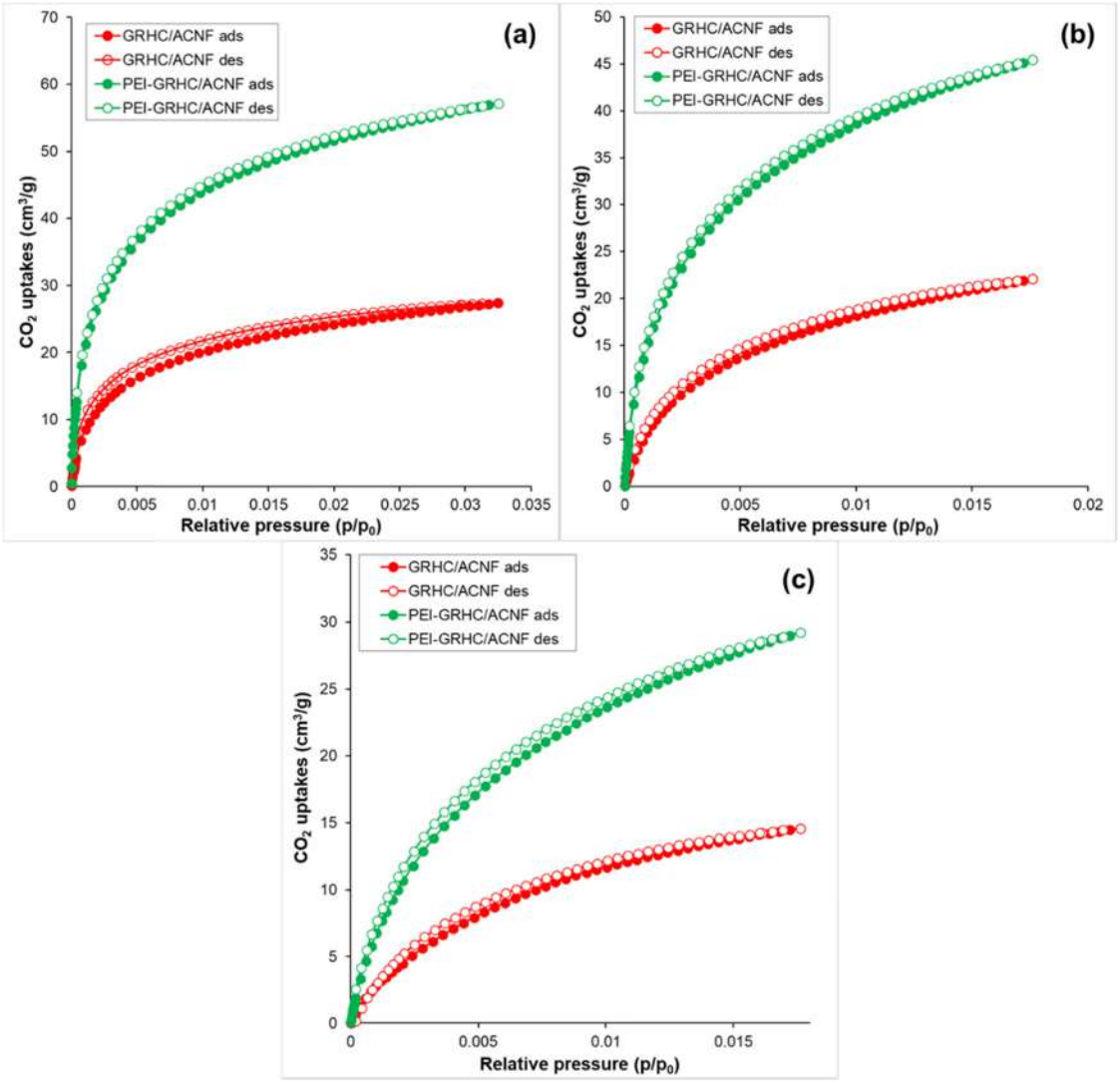

Figure 10: CO_2 adsorption/desorption on PEI-impregnated and nonimpregnated GRHC/ACNFs at different temperatures (a) 0°C; (b) 25°C; and (c) 50°C under atmospheric pressure.

CO_2 uptakes through chemisorption [71]. With low value of S_{BET} (presence of very low V_{meso} or macropores), it can be said that PEI does not totally block the surface of the GRHC/ACNFs leaving spaces for physisorption to take place. Both GRHC/ACNFs and PEI- GRHC/ACNFs show the highest CO_2 uptakes as compared with other samples as shown in Table 8. For further adsorption studies, both samples have been used and were denoted as PEI-GRHC/ACNFs for PEI-impregnated samples and GRHC/ACNFs for nonimpregnated ones.

Figure 10 shows the CO_2 adsorption isotherm of the GRHC/ACNFs and PEI-GRHC/ACNFs at atmospheric pressure and temperatures of 0°C, 25°C, and 50°C. Figure 10 reveals that the desorption of both impregnated and nonimpregnated samples at different temperatures shows no hysteresis. This means that both samples have very good adsorption/desorption capacity. It was also observed that CO_2 adsorption capacity reduces with increasing temperature for both samples. The adsorbed amount of CO_2 in PEI-GRHC/ACNFs and GRHC/ACNFs decreased from 522 to 142 cm^3/g and 293 to 69 cm^3/g, respectively. At higher temperature, the energized gas molecules were rapidly occupied on the GRHC/ACNFs surface, therefore, resulting in fewer CO_2 molecules captured [72]. Moreover, low equilibrium of CO_2 at higher temperature was also due to the exothermic nature of the adsorption [73].

Table 9 summarizes the kinetic studies of the PEI-GRHC/ACNFs and GRHC/ACNFs in order to determine the most fitted kinetics adsorption for the adsorption of CO_2. Based on the R^2 values, both GRHC/ACNFs samples are best fitted to the pseudo first-order kinetic model at low adsorption pressure of 1 bar by displaying greater R^2 value of 0.891 and 0.899. Meanwhile, the significantly low values of R^2 found in both samples in pseudo second-order kinetic model. This means that the CO_2 adsorption process of GRHC/ACNFs involved a physisorption phenomenon at low pressure as per our expectation, which means the physisorption is more related to the adsorption toward the surface with higher S_{BET}, TPV, and V_{micro} by weak dipole van der Waals interactions. These results are also in agreement with the results of S_{BET}, N_2, and CO_2 adsorption previously discussed. Remarkably, even though the nonimpregnated GRHC/ACNFs show the results as expected, however, the PEI-impregnated GRHC/ACNFs show result beyond our expectations as they also obeyed the pseudo first-order kinetic model. This is believed to be because of the small amount of amino groups presence in the impregnated samples (due to the low ratio of PEI:GRHC/ACNF:DI water; 1:1:5 used) that led to weaker interaction between PEI and CO_2 molecules resulting to minimum effects on the chemical interaction while involving physical interaction simultaneously [74]. In low pressure, physical interaction exhibits more dominant effect on the adsorption process. This is corresponding with previous study conducted by Liu *et al.* as they found that PEI-impregnated porous polymer-based adsorbents suggest both physical adsorption and chemical adsorption toward CO_2 [75].

Interestingly, at higher adsorption pressure of 15 bar, both samples can be ascribed by pseudo first-order and pseudo second-order kinetic models as the R^2 values obtained were high in both models. The R^2 values of pseudo first order of PEI-GRHC/ACNFs and GRHC/ACNFs are 0.7978 and 0.9154, respectively. Meanwhile, the R^2 values of pseudo second order of PEI-impregnated GRHC/ACNFs and nonimpregnated GRHC/ACNFs are 0.996 and 0.986, respectively. These findings indicate that the adsorption properties of both GRHC/ACNFs involve both chemical and physical reactions between the free active sites and open pores available on the GRHC/ACNFs and the CO_2 molecules. Moreover, this also confirms the main idea of PEI impregnation is to improve the CO_2 adsorption by introducing the basic N-functional groups onto the GRHC/ACNFs for better binding with acidic CO_2 molecules through chemisorption without cancelling the physisorption properties. To conclude, both kinetic models used in this study are suitable for the present data obtained for the adsorption of CO_2 at 15 bar and 25°C; however, it fits the best with pseudo second order and followed by pseudo first order [76].

Table 9: The fitted parameters of pseudo first order and pseudo second order of PEI-GRHC/ACNFs and GRHC/ACNFs at 1 and 15 bar

Sample	Pressure (bar)	$q_{e,\,exp}$ (cm^3/g)	Pseudo first order			Pseudo second order		
			k_1	$q_{e,cal}$	R^2	k_2	$q_{e,cal}$	R^2
GRHC/ACNF	1	142	−0.0414	3.05	0.899	0.0061	1.95	0.038
PEI-GRHC/ACNF		191	−0.0523	3.87	0.891	0.0305	11.82	0.257
GRHC/ACNF	15	522	−0.0343	4.13	0.915	0.1586	1.38	0.986
PEI-GRHC/ACNF		606	−0.0528	4.51	0.798	0.3865	2.71	0.996

Table 10: The fitted parameters of Langmuir, Freundlich, and BET isotherm models of PEI-GRHC/ACNFs and GRHC/ACNFs at 1 bar

Sample	Freundlich			Langmuir			BET
	n (mmol/g)	K_F	R^2	q_{max} (mmol/g)	K_L (bar^{-1})	R^2	R^2
GRHC/ACNF	0.785	2.434	0.841	8.688	39.179	0.999	0.987
PEI-GRHC/ACNF	0.761	2.339	0.810	6.379	27.073	0.998	0.972

Table 10 summarizes the linearized plot of the experimental data correlated to the Langmuir, Freundlich, and BET models to determine the homogeneity and heterogeneity energy distribution on the surface of the adsorbents. The R^2 values show that the resultant GRHC/ACNFs best fitted in Langmuir model and followed by BET. This implies that the adsorption of CO_2 involves monolayer phenomenon with homogeneous distribution on adsorbent active sites as previously discussed by Kim *et al.* [24]. In Langmuir isotherm and BET model, the dynamic equilibrium can be obtained by balancing the relative rates of adsorption and desorption based on the GRHC/ACNFs surface coverage [77].

It is believed that the adsorption process on the resultant GRHC/ACNFs does not only involve the formation of monolayer but also the formation of multilayers simultaneously [78]. This result was also supported by N_2 adsorption/desorption mentioned previously, in which the adsorption is monolayer at lower pressure but forming multilayers at higher pressures. This multilayer formation is best described by the Freundlich model. This model explains the adsorption process on surface adsorption sites which are energetically homogeneous.

Apart from a high CO_2 uptakes and fast adsorption/desorption kinetics, a good adsorbent should be stable and regenerated under mild conditions, in order to avoid high costs of the energy penalty. In this study, the cyclic behavior and stability of both impregnated and nonimpregnated GRHC/ACNFs were investigated *via* five consecutive CO_2 adsorption/desorption cycles for 14 h at 50°C (Figure 11). The selection of this adsorption temperature is to replicate the real condition of postcombustion CO_2 capture that is commonly used for adsorbent materials. As shown, there is a slight loss in adsorption capacity after each cycle. After five cycles, the stability of the impregnated GRHC/ACNFs shows almost similar drop percentage of 23% (from 32.2 to 24.6 cm^3/g) as compared with nonimpregnated GRHC/ACNFs of 22% (15.1–11.8 cm^3/g). This is could possibly be due to imperfect regeneration of the adsorbents due to the high affinity of PEI toward CO_2 and the current desorption method is insufficient to evacuate all CO_2 from the adsorbents. Moreover, PEI-modified ACNFs are dominated by chemisorption, and hence require higher energy (*i.e.* temperature) to evacuate CO_2. It has been found that this dropping percentage is considered acceptable for amine-impregnated samples after five cycles, as the capacity of the carbon capture under the same conditions on tetraethylenepentamine (TEPA) impregnated electrospun carbon nanofibers by a study conducted by Wang *et al.* [79] reported the drop is more than 11%. Rather than its higher drop percentage as compared with previously reported studies, the GRHC/ACNFs possessed comparable or superior adsorption capacity over other samples which is up to 27.1 cm^3/g at 50°C. Even though the GRHC/ACNFs obtained in this study do not show similar adsorption capacity compared with the first cycle, however it become more stable from the fourth cycle to fifth cycle, which shows that the percentage drop is very low. It has been found that the resultant GRHC/ACNFs have good recyclability as well as mild regeneration conditions, which is believed to have high potential for practical applications in energy-efficient carbon capture processes.

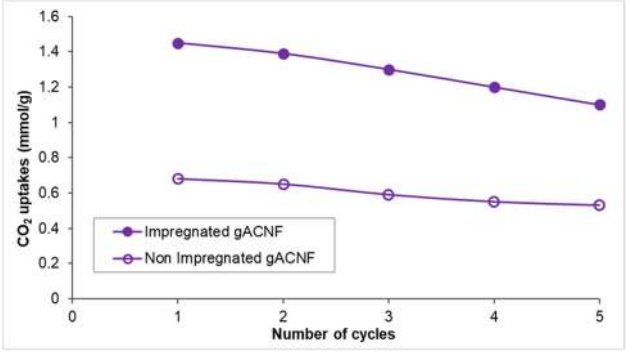

Figure 11: Cyclic ability of the CO_2 adsorption on PEI-impregnated and nonimpregnated GRHC/ACNFs at 50°C and 1 bar.

4 Conclusion

In conclusion, it can be said that the physicochemical properties of the pristine ACNFs and their adsorption performances can be improved by suitable loading of additives or nanofillers. In this study, it has been found that graphene-based materials such as GRHC could

greatly enhance the properties of the pristine ACNFs, especially in terms of their porosity and textural properties that were the major contributing factors for their excellent CO_2 adsorption capacity. GRHC, which shows high S_{BET} as well as good electrical conductivity, produced in this study has been used as additive to improve the solution conductivity during the electrospinning process, which helps in producing fiber with smaller diameter. This is because the adsorption capacity is highly dependent upon the S_{BET}, TPV, and V_{micro} of the adsorbents; the higher the S_{BET} and V_{micro}, the higher the adsorption capacity. Compared with pristine ACNFs, GRHC/ACNFs exhibited better porous properties and consequently, exhibited the highest adsorption capacity toward CO_2—up to 142.1 cm^3/g. Meanwhile, the adsorption capacity of the samples was enhanced by impregnating amine-based chemicals, such as PEI, onto the ACNFs and GRHC/ACNFs. The presence of amine groups in PEI-impregnated samples enhanced the chemical interaction between the basic properties of amines and acidic properties of CO_2 adsorbates. The adsorption capacity in PEI-GRHC/ACNFs composites was found to be the highest with the value of 190.9 cm^3/g under atmospheric pressure and 25°C. This is could possibly be due to the interaction of both physical and chemical adsorption that simultaneously occurred and resulted in high CO_2 adsorption.

Acknowledgements: The authors would like to acknowledge the financial support from the Malaysian Ministry Education and Universiti Teknologi Malaysia under the UTM Prototype Research grant (UTMPR) (Q.J130000.2851.00L41); collaborative research grant (CRG) (Q.J130000.2451.087G72) and (Q.J130000.2451.08G26); UTM-TDR grant scheme (Q.J130000.3551.06G07); HICOE research grant (R.J090 301.7851.4J428), and Professional Development Research University grant (Q.J130000.21A2.05E42). The work was carried out through the financial support of the Ministry of Education, Youth and Sports of the Czech Republic and the European Union (European Structural and Investment Funds – Operational Programme Research, Development and Education) under the project "Modular platform for autonomous chassis of specialized electric vehicles for freight and equipment transportation," Reg. No. CZ.02.1.01/0.0/0.0/16_025/0007293. The authors would also like to acknowledge the technical and management support from the Research Management Centre, Universiti Teknologi Malaysia (RMC, UTM). One of the authors, Othman, F.E.C. would like to acknowledge the Zamalah scholarship received from UTM, NIMS Internship Scholarship 2018 awarded by the National Institute for Materials Science (NIMS), Japan, and the Mitacs-Globalink Research Award 2020 awarded by Mitacs and Ecole Polytechnique de Montreal, Canada.

Funding information: Malaysian Ministry Education and Universiti Teknologi Malaysia under the UTM Prototype Research grant (UTMPR) (Q.J130000.2851.00L41); collaborative research grant (CRG) (Q.J130000.2451.087G72) and (Q.J130000.2451.08G26); UTM-TDR grant scheme (Q.J13 0000.3551.06G07); HICOE research grant (R.J090301.7851. 4J428) and Professional Development Research University grant (Q.J130000.21A2.05E42). The work was carried out through the financial support of the Ministry of Education, Youth and Sports of the Czech Republic and the European Union (European Structural and Investment Funds – Operational Programme Research, Development and Education), Reg. No. CZ.02.1.01/0.0/0.0/16_025/0007293.

Author contributions: All authors have accepted responsibility for the entire content of this manuscript and approved its submission.

Conflict of interest: The authors state no conflict of interest.

References

[1] Mondal MK, Balsora HK, Varshney P. Progress and trends in CO_2 capture/separation technologies: a review. Energy. 2012;46(1):431–41.

[2] Mauna Lao Lab. Global Monitoring Laboratory – Carbon Cycle Greenhouse Gases. US Department of Commerce, NOAA, Global Monitoring Laboratory Accessed on November 6, 2020 from https://www.esrl.noaa.gov/gmd/ccgg/trends/.

[3] Global Greenhouse Gas Emissions by United States Environmental Protection Agency (EPA). Accessed on November 06, 2020 from https://www.epa.gov/ghgemissions/global-greenhouse-gas-emissions-data.

[4] Ammendola P, Raganati F, Chirone R, Miccio F. Fixed bed adsorption as affected by thermodynamics and kinetics: yellow tuff for CO_2 capture. Powder Technol. 2020;373:446–58.

[5] Megías-Sayago C, Bingre R, Huang L, Lutzweiler G, Wang Q, Louis B. CO_2 adsorption capacities in zeolites and layered double hydroxide materials. Front Chem. 2019;7(51):1–10.

[6] Wang K, Shang H, Li L, Yan X. Efficient CO_2 capture on low-cost silica gel modified by polyethyleneimine. J Nat Gas Chem. 2012;21(3):319–23.

[7] Creamer AE, Gao B. Carbon-based adsorbents for postcombustion CO_2 capture: a critical review. Environ Sci Technol. 2016;50(14):7276–89.

[8] Hu Z, Wang Y, Shah BB, Zhao D. CO_2 capture in metal-organic framework adsorbents: an engineering perspective. Adv Sustain Syst. 2018;3(1):1800080.

[9] Othman FEC, Yusof N, Hasbullah H, Jaafar J, Ismail AF, Abdullah N, et al. Polyacrylnitrile/magnesium oxide-based activated carbon nanofibers with well-developed microporous structure and their adsorption performance for methane. J Ind Eng Chem. 2017;51:281–7.
[10] Othman FEC, Yusof N, González-Benito J, Fan X, Ismail AF. Electrospun composites made of reduced graphene oxide and polyacrylonitrile-based activated carbon nanofibers (rGO/ACNF) for enhanced CO_2 adsorption. Polymers. 2020;12(9):1–19.
[11] Rouzitalab Z, Maklavany DM, Rashidi A. Synthesis of N-doped nanoporous carbon from walnut shell for enhancing CO_2 adsorption capacity and separation. J Environ Chem Eng. 2018;6:6653–63.
[12] Raganati F, Miccio F, Ammendola P. Adsorption of carbon dioxide for post-combustion capture: a review. Energy Fuels. 2021;35:12845–68.
[13] Othman FEC, Yusof N, Ismail AF, Jaafar J, Salleh WNW, Aziz F. Preparation and characterization of polyacrylonitrile-based activated carbon nanofibers/graphene (gACNFs) composite synthesized by electrospinning. AIP Adv. 2020;10:055117.
[14] Othman FEC, Ismail MS, Yusof N, Samitsu S, Yusop MZ, Ariffin NFT, et al. Methane adsorption by porous graphene-derived from rice husks ashes under various stabilization temperatures. Carbon Lett. 2020;30(5):535–43.
[15] Othman FEC, Yusof N, Ismail AF. Activated carbon nanofibers/graphene nanocomposites and their adsorption performance towards carbon dioxide. Chem Eng Tech. 2020;43(10):2023–30.
[16] Romano MC, Anantharaman R, Arasto A, Ozcan DC, Ahn H, Dijkstra J, et al. Application of advanced technologies for CO_2 capture from industrial sources. Energy Procedia. 2013;37:7176–85.
[17] Romero JRG, Moreno-Piraján JC, Giraldo L. Kinetic and equilibrium study of the adsorption of CO_2 in ultramicropores of resorcinol-formaldehyde aerogels obtained in acidic and basic medium. J Carbon Res C. 2018;4:52.
[18] Khalil SH, Aroua MK, Daud WMAW. Study on the improvement of the capacity of amine-impregnated commercial activated carbon bed for CO_2 adsorbing. Chem Eng J. 2012;183:15–20.
[19] Qi L, Tang X, Wang Z, Peng X. Pore characterization of different types of coal and gas outburst disaster sites using low temperature nitrogen adsorption approach. Int J Min Sci Technol. 2017;37:371–7.
[20] Lee SY, Park SJ. Determination of the optimal pore size for improved CO_2 adsorption in activated carbon fibers. J Colloid Interface Sci. 2013;389:230–5.
[21] Sing KS, Williams RT. Physisorption hysteresis loops and the characterization of nanoporous materials. Adsorpt Sci Technol. 2004;22:773–82.
[22] Liu H, Ding W, Lei S, Tian X, Zhou F. Selective adsorption of CH_4/N_2 on Ni-based MOF/SBA-15 composite materials. J Nanomater. 2019;9(149):1–14.
[23] Nasrollahzadeh M, Babaei F, Fahkri P, Jaleh B. Synthesis, characterization, structural, optical properties and catalytic activity of reduced graphene oxide/copper nanocomposites. RSC Adv. 2015;5:10782–89.
[24] Kim DW, Jung DW, Adelodun AA, Jo YM. Evaluation of CO_2 adsorption capacity of electrospun carbon fibers with thermal and chemical activation. J Appl Polym Sci. 2017;134:45534.
[25] Lee HM, Kang HR, An KH, Kim HG, Kim BJ. Comparative studies of porous carbon nanofibers by various activation methods. Carbon Lett. 2012;14(3):180–5.
[26] Manoj B, Kunjomana AG. Study of stacking structure of amorphous carbon by X-ray diffraction technique. Int J Electrochem Sci. 2012;3127–34.
[27] Ouassim B, Fouad G, Arunabh G, Ouafae A, Tarik C. Excellent CO_2 capture by ultra-high microporous activated carbon made out from Natural coal. Chem Eng Technol. 2020;44(1):148–55.
[28] Huang G, Liu Y, Wu X, Cai J. activated carbons prepared by the KOH activation of a hydrochar from garlic peel and their CO_2 adsorption performance. New Carbon Mater. 2019;34:247–57.
[29] Mishra AK, Ramaprabhu S. Carbon dioxide adsorption in graphene sheets. AIP Adv. 2011;1:032152.
[30] Guo B, Chang L, Xie K. Adsorption of carbon dioxide on activated carbon. J Natur Gas Chem. 2006;25:223–38.
[31] Gayathri S, Jayabal P, Kottaisamy M, Ramakrishnan V. Synthesis of few layers graphene by direct exfoliation of graphite and a Raman spectroscopic study. AIP Adv. 2014;4:027116.
[32] Pei S, Cheng HM. The reduction of graphene oxide. Carbon. 2012;50:3210–28.
[33] Hong SM, Kim SH, Jeon BG, Jo SM, Lee KB. Development of porous carbon nanofibers from electrospun polyvinylidene fluoride for CO_2 capture. RSC Adv. 2014;4:58956–63.
[34] Ali N, Babar AA, Zhang Y, Iqbal N, Wang X, Yu J, et al. Porous, flexible, and core-shell structured carbon nanofibers hybridized by tin oxide nanoparticles for efficient carbon dioxide capture. J Colloid Interface Sci. 2020;560:379–87.
[35] Huang ZM, Zhang YZ, Kotaki M, Ramakrishna S. A review on polymer nanofibers by electrospinning and their applications in nanocomposites. Compos Sci Technol. 2003;63:2223–53.
[36] Li JH, Zhang GH, Wang Z. CO_2 absorption of powdered $Ba_2Fe_2O_5$ with different particle size. High Temp Mater Process. 2018;37(9–10):1001–6.
[37] Yadav D, Amini F, Ehrmann A. Recent advances in carbon nanofibers and their applications – a review. Eur Polym J. 2020;138:109963.
[38] Pu X, Yang X, Zhang Y, Li L, Xie Y, He B, et al. Fabrication and characterization of highly oriented composite nanofibers with excellent mechanical strength and thermal stability. Macromol Mater Eng. 2020;305:1900691.
[39] Cychosz KA, Guillet-Nicolas R, Garcia-Martinez J, Thommes M. Recent advances in the textural characterization of hierarchically structured nanoporous materials. Chem Soc Rev. 2017;46(2):389–414.
[40] Cychosz KA, Thommes M. Progress in the physisorption characterization of nanoporous gas storage materials. Eng. 2018;4:559–66.
[41] Martin CF, Sweatman MB, Brandani S, Fan X. Wet impregnation of a commercial low-cost silica using DETA for a fast post-combustion CO_2 capture process. Appl Energy. 2016;183:1705–21.
[42] Bai G, Han Y, Du P, Fei Z, Chen X, Zhang Z, et al. Polyethyleneimine (PEI)-impregnated resin adsorbent with high efficiency and capacity for CO_2 capture from flue gas. New J Chem. 2019;43(46):18345–54.
[43] Fu X. Polyethyleneimine-silica mesoporous hybrid: a novel adsorbent for CO_2 capture. Adv Compos Lett. 2012;21(2):37–43.

[44] Wang X, Li G, Seo MH, Lui G, Han FM, Feng K, et al. Carbon-coated silicon nanowires on carbon fabric as self-supported electrodes for flexible lithium-ion batteries. ACS Appl Mater Interfaces. 2017;9:9551–8.
[45] Zeeshan M, Yalcin K, Oztuna FES, Unal U, Keskin S, Uzun A. A new class of porous materials for efficient CO_2 separation: ionic liquid/graphene aerogel composites. Carbon. 2021;171:79–87.
[46] Lee SY, Park SJ. Preparation and characterization of ordered porous carbons for increasing hydrogen storage behaviors. J Solid State Chem. 2011;184(10):2655–60.
[47] Ullah S, Shariff AM, Bustam MA, Elkhalifah AEI, Murshid G, Riaz N, et al. Modified MIL-53 with multi-wall carbon nanotubes and nanofibers on CO_2 adsorption. Appl Mech Mater. 2014;625:870–3.
[48] Ojeda-López R, Esparza-Schulz JM, Perez-Hermosillo IJ, Hernandez-Gordillo A, Dominguez-Ortiz A. Improve in CO_2 and CH_4 adsorption capacity on carbon microfibers synthesized by electrospinning of PAN. Fibers. 2019;7:81.
[49] Meng LY, Park SJ. Effect of heat treatment on CO_2 adsorption of KOH-activated graphite nanofibers. J Colloid Interface Sci. 2010;352:498–503.
[50] Yuan H, Meng LY, Park SJ. KOH-activated graphite nanofibers as CO_2 adsorbents. Carbon Lett. 2016;19:99–103.
[51] Iqbal N, Wang X, Babar AA, Yu J, Din B. Highly flexible $NiCo_2O_4$/CNTs doped carbon nanofibers for CO_2 adsorption and supercapacitor electrodes. J Colloid Interface Sci. 2016;476:87–93.
[52] Nan D, Liu J, Ma W. Electrospun phenolic resin-based carbon ultrafine fibers with abundant ultra-small micropores for CO_2 adsorption. Chem Eng J. 2015;276:44–50.
[53] Aksoylu AE, Madalena M, Freitas A, Pereira MFR, Figueiredo JL. The effects of different activated carbon supports and support modifications on the properties of Pt/AC catalysts. Carbon. 2010;39:175–85.
[54] Gomes HT, Machado BF, Ribeiro A, Moreira I, Rosario M, Silva AMT, et al. Catalytic properties of carbon materials for wet oxidation of aniline. J Hazard Mat. 2008;159:420–6.
[55] Diez N, Alvarez P, Granda M, Blanco C, Santamaria R, Menendez R. A novel approach for the production of chemical activated carbon fibers. Chem Eng J. 2015;114:2243–51.
[56] Titinchi SJJ, Piet M, Abbo HS, Bolland O, Schwieger W. Chemically modified solid adsorbents for CO_2 capture. Energy Procedia. 2014;63:8153–60.
[57] Kishor R, Ghoshal AK. Amine-modified mesoporous silica for CO_2 adsorption: the role of structural parameters. Ind Eng Chem Res. 2017;56:6078–87.
[58] Chen C, Ahn W-S. 'CO_2 capture using mesoporous alumina prepared by a sol-gel process'. Chem Eng J. 2011;166(2):646–51.
[59] Pellerano M, Pre P, Kacem M, Delebarre A. CO_2 capture by adsorption on activated carbons using pressure modulation. Energy Procedia. 2009;1:647–53.
[60] Siriwardane RV, Shen MS, Fisher EP. Adsorption of CO_2 on zeolites at moderate temperatures. Energy Fuels. 2005;19(3):1153–9.
[61] Dawson R, Stockel E, Holst JR, Adams DJ, Cooper AI. Microporous organic polymers for carbon dioxide capture. Energy Environ Sci. 2011;4:4239–45.
[62] Vilarrasa-Garcia E, Cecilia JA, Azevedo DCS, Cavalcante Jr CL, Rodriguez-Castellon E. Evaluation of porous clay heterostructures modified with amine species as adsorbent for the CO_2 capture. Micropor Mesopor Mat. 2017;249:25–33.
[63] Ngoy JM, Wagner N, Riboldi L, Bolland O. A CO_2 capture technology using multiwalled carbon nanotubes with polyaspartamide surfactant. Energy Procedia. 2014;63:2230–48.
[64] Tan YL, Islam MA, Asif M, Hameed BH. Adsorption of carbon dioxide by sodium hydroxide-modified granular coconut shell activated carbon in a fixed bed. Energy. 2014;77:926–31.
[65] Shen C, Grande CA, Li P, Yu J, Rodrigues AE. Adsorption equilibria and kinetics of CO_2 and N_2 on activated carbon beads. Chem Eng J. 2010;160:398.
[66] Bikshapathi M, Sharma A, Sharma A, Verma N. Preparation of carbon molecular sieves from carbon micro and nanofibers for sequestration of CO_2. Chem Eng Res Des. 2011;89:1737–46.
[67] Choma J, Osuchowski L, Marszewski M, Dziura A, Jaroneic M. Developing microporosity in Kevlar1-derived carbon fibers by CO_2 activation for CO_2 adsorption. J CO_2 Util. 2016;16:17–22.
[68] Lee SY, Park SJ. Preparation and characterization of orderous porous carbons for increasing hydrogen storage behaviors. J Solid State Chem. 2011;184(10):2655–60.
[69] Chowdhury S, Parshetti GK, Balasubramaniam R. Post-combustion CO_2 capture using mesoporous TiO_2/graphene oxide nanocomposites. Chem Eng J. 2015;263:374–84.
[70] Li D, Ma T, Zhang R, Tian Y, Qiao Y. Preparation of porous carbons with high low-pressure CO_2 uptake by KOH activation of rice husk char. Fuels. 2015;139:68–70.
[71] Sanz R, Calleja G, Arencibia A, Sanz ES. Development of high efficiency adsorbents for CO_2 capture based on a double-functionalization method of grafting and impregnation. J Phys Chem A. 2012;1:1956–62.
[72] Builes S, Sandler SI, Xiong R. Isosteric heats of gas and liquid adsorption. Langmuir. 2013;29:10416–22.
[73] Singh VK, Kumar EA. Measurement and analysis of adsorption isotherms of CO_2 on activated carbon. Appl Therm Eng. 2016;97:77–86.
[74] Kong X, Li S, Stromme M, Xu C. Synthesis of porous organic polymers with tunable amine loadings for CO2 capture: balanced physisorption and chemisorption. Nanomater. 2019;9(7):1–11.
[75] Liu F, Chen S, Gao Y. Synthesis of porous polymer based solid amine adsorbent: effect of pore size and amine loading on CO_2 adsorption. J Colloid Interface Sci. 2017;506:236–44.
[76] Guo B, Wang Y, Shen X, Qiao X, Jia L, Xiang J, et al. Study on CO_2 capture characteristics and kinetics of modified potassium-based adsorbents. Mater. 2020;13(4):877.
[77] Ayawei N, Ebelegi AN, Wankasi D. Modelling and interpretation of adsorption isotherm. J Chem. 2017;1–11.
[78] Hu Y, Zhu Y, Zhang Y, Lin T, Zeng G, Zhang S, et al. An efficient adsorbent: simultaneous activated and magnetic ZnO doped biochar derived from camphor leaves for ciprofloxacin adsorption. Bioresour Technol. 2019;288:121511.
[79] Wang J, Adelodun AA, Oh JM, Jo YM. TEPA impregnation of electrospun carbon nanofibers for enhanced low-level CO_2 adsorption. Nano Converg. 2020;7(7):1–11.